

HHC-36 antimicrobial peptide loading on silk fibroin (SF)/hydroxyapatite (HA) nanofibrous-coated titanium for the enhancement of osteoblast and bactericidal functions

Nastaran Abbasizadeh, Ali Hossein Rezayan, Jhamak Nourmohammadi & Mehdi Kazemzadeh-Narbat

To cite this article: Nastaran Abbasizadeh, Ali Hossein Rezayan, Jhamak Nourmohammadi & Mehdi Kazemzadeh-Narbat (2019): HHC-36 antimicrobial peptide loading on silk fibroin (SF)/hydroxyapatite (HA) nanofibrous-coated titanium for the enhancement of osteoblast and bactericidal functions, International Journal of Polymeric Materials and Polymeric Biomaterials, DOI: [10.1080/00914037.2019.1596913](https://doi.org/10.1080/00914037.2019.1596913)

To link to this article: <https://doi.org/10.1080/00914037.2019.1596913>



Published online: 12 Apr 2019.



Submit your article to this journal [↗](#)



View Crossmark data [↗](#)

HHC-36 antimicrobial peptide loading on silk fibroin (SF)/hydroxyapatite (HA) nanofibrous-coated titanium for the enhancement of osteoblast and bactericidal functions

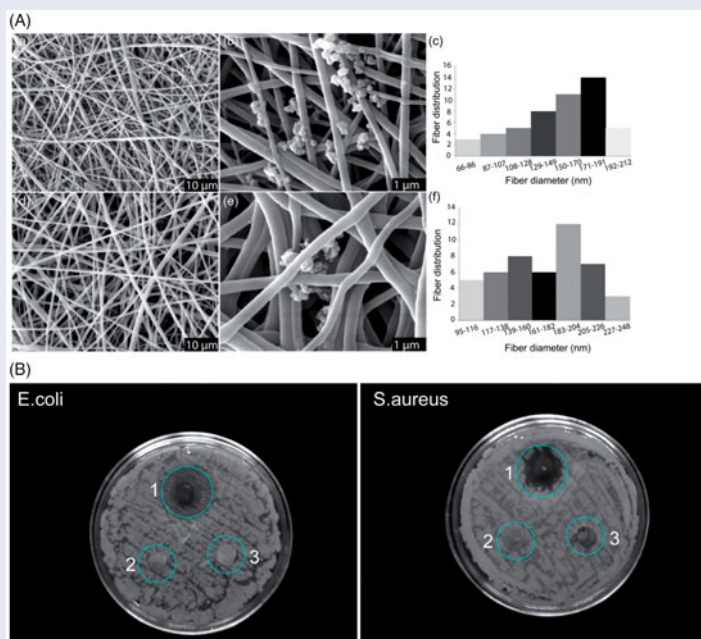
Nastaran Abbasizadeh^a, Ali Hossein Rezayan^a, Jhamak Nourmohammadi^a, and Mehdi Kazemzadeh-Narbat^b

^aDepartment of Life Science Engineering, Faculty of New Sciences and Technologies, University of Tehran, Tehran, Iran; ^bBiomaterials Innovation Research Center, Division of Biomedical Engineering, Department of Medicine, Brigham and Women's Hospital, Harvard Medical School, Boston, MA, USA

ABSTRACT

Improving osseointegration together with preventing infections are the main challenges of using titanium-based implants in joint replacement surgeries. In this study, a hybrid composite of silk fibroin (SF)/hydroxyapatite (HA) nanofibrous mats was directly electrospun on titanium plates in order to mimic the bone extracellular structure and improve osteoconductivity. Afterwards, HHC-36 antimicrobial peptide (AMP) was immobilized on the fabricated mats using dopamine as a linker. The morphology, bioactivity, and adhesive strength of the coating were characterized, and the cellular responses and antimicrobial activity of the modified titanium plates were assessed. The results exhibited a strong interfacial attachment and homogeneously dispersed HA nanoparticles in the electrospun nanofibers. No cytotoxicity was observed for MG-63 cells and the coating could effectively induce cell differentiation. The cumulative release profile of HHC-36 showed a burst release within first 3 h, followed by a slow and steady release over 48 h. Finally, AMP could eradicate the representative Gram-positive and Gram-negative bacteria within 3 h while maintaining the antimicrobial activity for up to 21 days.

GRAPHICAL ABSTRACT



(A) The SEM morphology and fiber diameter distribution of electrospun SF/HA nanofibers after modification with (a,b,c) PDA and (d,e,f) HHC-36, and (B) Assessing the antibacterial activity of (1) Ti/SF/HA/AMP (2) Ti/SF/HA and (3) Ti against *E. coli* and *S. aureus* by Disk Diffusion test

ARTICLE HISTORY

Received 21 December 2018
Accepted 14 March 2019

KEYWORDS

Antimicrobial peptide;
hydroxyapatite
nanoparticles; silk fibroin
fibers; titanium implant

1. Introduction

Nowadays, cementless joint replacements have gained much attention for the surgery of arthritic diseases of the hip and knee joints^[1]. Among metallic implants, titanium (Ti) and its alloys are frequently used as orthopedic implants because of their excellent biocompatibility, high specific strength, low elastic modulus, and great corrosion resistance^[1–5]. Unfortunately, despite of these characteristic features, Ti-based implants are not bioactive and show less osteointegration with their surrounding bone, which lead to implant migration and consequently loosening of implants^[6, 7]. Various surface modifications have been developed to improve osteointegration and one of the most common ones is coating the Ti surface with calcium phosphate and hydroxyapatite (HA)^[6, 8]. Recently, using composites of nanofibrous biopolymers/HA has gained much attention due to its similarity to the bone extra cellular matrix (ECM) and providing large surface area, which can result in enhanced cellular responses^[9–11]. Among biopolymers, silk fibroin is widely studied in bone regeneration applications by reason of its unique properties such as structural integrity, biocompatibility, controllable degradation rate, low inflammatory response, and having the RGD sequences improving cell responses^[12–14]. Therefore, it seems that directly co-electrospinning of SF and HA on Ti, which has not been investigated yet, to the best of our knowledge, can be a potential candidate for improving osteointegration of Ti.

Another complication that threatens the osteointegration and may cause of failure in orthopedic implants and increase of patient morbidity is pre-implant associated infection. The surface of Ti implants is very vulnerable to adhesion, colonization, and biofilm formation of bacteria. This may compromise immune ability at the implant/tissue interface, which triggers infections^[15–18]. The treatment of such infections is usually very difficult because the bacteria in biofilm are 10 to 1000 times less susceptible to the host immune system and are protected by biofilm from antibiotic penetration^[19–21]. In this case the removal and replacement of the prosthesis might be the last remedy^[16, 22, 23]. One solution to combat the biofilm formation is localized delivery of antimicrobial agents such as gentamicin, vancomycin, and cephalothin at the site of implants^[18, 19]. However, the emergence of superbugs and multi-drug resistant organisms such as methicillin-resistant *Staphylococcus aureus* (MRSA) has critically challenged the efficacy of conventional antibiotics^[20]. On the other side, due to long-term cytotoxicity as well as low efficiency limitations, coating the implant surfaces with non-antibiotic drugs such as silver compounds has not been successful^[18]. Short cationic antimicrobial peptides (AMPs) are new generation of antimicrobial agents with strong antibacterial activity, which can be a suitable alternative to conventional antibiotics^[24, 25]. Unique characteristics of AMPs such as wide spectrum bactericidal activity, and potency against drug-resistant microorganisms, viruses, fungus and, parasites have attracted a lot of attention recently^[25–27]. AMPs are relatively short, consist of cationic, and amphiphilic amino acids, which kill bacteria rapidly via

binding with the negatively charged phospholipids layers in bacteria membrane^[28–30]. HHC-36AMP as one of the most potent short AMPs and with a flexible structural shape has two positive features distinguishing it from other AMPs. The first one is related to the HHC-36 MICs (0.3 to 11 μM) which are much more less than general MICs (10–76 μM) that are being used and the second one is low cytotoxicity of HHC-36 in a metabolically active cell and minimal red bloodcell lysis for concentrations more than 251 μM ^[31–33]. Despite these advantages, there are few studies on using HHC-36 for suppressing infections of orthopedic biomaterials. Kazemzadeh et.al suggested HHC-36/CaP as a good candidate for enhancing osteoconductivity and antibacterial activity both *invitro* and *in vivo*^[22]. These properties indicate that coating HHC-36 along with SF/HA nanofibrous mats on Ti would serve as a good candidate to improve osteointegration and reduce implant-associated infections, which has not been studied yet.

Reports concerning immobilizing the AMPs on biomaterial surfaces have stated that long and flexible spacer between AMPs and surfaces is necessary to improve the bactericidal activity of AMP^[18, 34]. Self-assembled silane monolayers^[35] and layer-by-layer assembly^[20] are amongst the efforts to immobilize AMPs on biomaterials surfaces. However, these methods need complicated chemical modification and are limited to specific samples^[36]. Also there are some evidences that show co-electrospinning of AMP with polymers has some clinical implications because of their linear release profile and lack of uniform distribution throughout the fibers^[37]. In this view, two aforementioned protocols of immersing and co-electrospinning of AMP with SF/HA matrices were done too, but AMP release profile and antimicrobial tests rejected the effectiveness of these approaches.

In continuation of our interest in the synthesis of nanomaterials and investigation of their application in diagnosis and treatment^[19, 20, 22, 38–41], the aim of this study is introduction a unique strategy for local delivery of HHC-36 from nanofibrous mats of SF/HA coated on Ti. Regard to this, we used a new approach of using Poly Dopamine (PDA) as a linker to immobilize the AMP and provide a bactericidal coating on Ti surface. Recently, this strategy has gained much attention due to covalently bind proteins to different substrates via Michael reaction^[42, 43]. For this purpose, SF/HA nanofibrous mats were co-electrospun directly on the Ti plates, followed by the conjugation of the HHC-36 on the electrospun hybrid SF/HA composite mats by using PDA. Several characterization techniques were done in order to evaluate the morphology, bioactivity, and adhesive strength between Ti and electrospun mats. In addition, the *in vitro* cellular response and antimicrobial activities were tested on the coated substrates.

2. Experimental

2.1. Material

HHC-36 (KRWKWWRR) with the purity of 95% was obtained from MIMITOPES, Australia. Cocoons of *Bombyxmori* (*B. mori*) were obtained from the Iranian

silkworm research center. Besides, Sodium carbonate, lithiumbromide, Methanol, Ethanol, Acetone, Hydrofluoric acid, Nitric acid, formic acid, Calcium hydroxide, Phosphoric acid, Hydrochloric acid, Cellulose dialysis cassette, Glutaraldehyde 25%, Ammonia, Disodium phosphate, Sodium Hydroxide, Dopamine hydrochloride, and Tris-HCl were purchased.

2.2. Synthesis and characterization of nano-hydroxyapatite (n-HA)

Generally, HA is synthesized either by solid state reactions or wet chemistry methods^[44]. In the present work HA was synthesized by wet chemical precipitation reaction between H_3PO_4 and $Ca(OH)_2$ ^[45]. Briefly, 0.5 M calcium hydroxide $Ca(OH)_2$ powder was added into deionized water and then 0.3 M phosphoric acid (H_3PO_4) solution was transferred drop wise (one to two drops per second) into calcium hydroxide solution. During precipitation process, the pH was adjusted to pH = 10 by adding NH_4OH solution. The solution was rested at 37 °C for 24 h until precipitate was formed. Subsequently the precipitate was washed three times with deionized water and dried at 75 °C in the oven. The powder was milled and then passed through a sieve (200 mesh) to form HA nanoparticles. Analysis of HA nanoparticles morphology, phase and size were carried out using field emission scanning electron microscopy. Drop of nano-HA suspension was put on the slab and allowed to dry and finally was sputtered with gold. Afterward, The Ca/P ratio of HA nanoparticles was analyzed by energy-dispersive X-ray spectroscopy.

2.3. Preparation of silk fibroin solutions

Silk fibroin was extracted from *B. mori* Cocoons based on our previous study^[46]. Briefly, chopped cocoons were boiled in an aqueous solution of 5% Na_2CO_3 at 100 °C for 45 min. Then degummed cocoons were rinsed with water to extract sericin and allowed to dry in the oven at 37 °C for 24 h. Afterward, the obtained SF was dissolved in 3.9 M lithium bromide (LiBr) solution at 60 °C for 4 h and finally dialyzed against deionized water to remove LiBr. After 3 days, the solution was stored in -20 °C for 24 h and then freeze-dried.

2.4. Preparation of SF/HA electrospun nanofiber

Prior to electrospinning, Ti plates ($1 \times 1 \times 0.5 \text{ cm}^3$) were ground with 320 grit sandpaper and then washed in ethanol 70% and soap for 15 min to remove organic contaminant followed by washing with distilled water and acetone for 10 min. Cleaned Ti samples were etched in mixture of 2% hydrofluoric acid (HF) and 36% HNO_3 for 30 s at room temperature. Then specimens were taken out, rinsed thoroughly with ethanol and distilled water and dried at 50 °C in an oven.

SF solution was prepared by dissolving 0.13 g SF sponges and 1 mg HA nanoparticles in 1 ml formic acid and stirring

for at least 3 h at room temperature. We tested different ratios of HA/SF (0.5%, 1%, 2%, 3%) and after doing different characterization and cellular test, this ratio was chosen as the best one. The solution was loaded into the syringe of the electrospinning apparatus. The process was carried out at 15 kV, under flow rate 0.5 ml/h, and the distance between the tip of syringe and Ti (collector) was set to 13 cm. These parameters have been determined based on our previous projects. At first, we put the basic parameters based on the data of this article and then change them to a little extent to reach nanofibers with the minimum beads and reasonable diameter.

2.5. Characterization of SF/HA electrospun nanofibers

The surface morphology and fibers diameter of the electrospun SF/HA were examined using SEM after the specimens were gold sputter coated. To determine the average diameter of fibers and their distribution, 50 random fibers were measured by Image-J software. In order to investigate the distribution of HA nanoparticles integrated into the SF nanofibers, the EDX was utilized. To confirm the presence of HA in the SF nanofibers, Fourier Transform Infrared spectroscopy was used. In addition, the adhesion strength between SF/HA nanofibers and Ti was measured by pull-Off method in accordance with ASTM D4541.

2.6. Immobilizing and characterization of AMP loaded coating

To immobilize AMP onto the SF/HA nanofibers coated Ti plates, the coating was first modified with PDA and subsequently HHC-36 was conjugated onto the PDA-coated surface. It is noteworthy that before implementing this method, different protocols of immersing, co-electrospinning of AMP with SF/HA matrices, and layer-by-layer cationic poly(allylamine hydrochloride) (PAH) and anionic poly(acrylic acid)(PAA) modifications were testified, but AMP release profile and antimicrobial tests didn't show promising results (data not shown). Anyway, to modify the implants with PDA, the Ti plates coated with electrospun SF/HA were immersed into 1.0 ml of dopamine solution (5.0 mg ml^{-1} , in 50 mM Tris-HCl, pH 8.8) for 4 days at 25 °C^[33]. Afterwards, the plates were washed thoroughly with deionized water to remove unattached PDA and then dried at room temperature. Fifty micro liter of the HHC-36 solution in ethanol (1 mg ml^{-1}) was pipetted on the PDA-coated plates and allowed to dry in vacuum oven for 15 min at 37 °C. This process was repeated three times^[20]. Finally, the samples were rinsed with 1 ml phosphate buffer saline (PBS) and dried at room temperature. The surface morphology of the electrospun fibers after modification with PDA and AMP was observed by SEM. The wet ability of surfaces was measured using static water contact angle by the sessile drop method. For each sample, the water contact angle value was reported as the results of three water droplets ($4 \mu\text{l}$) ($n = 3$).

2.7. In vitro AMP release

The *in vitro* release of AMP was examined at different time points using Ultraviolet–Visible spectroscopy (UV-Vis) based on previous study of Kazemzadeh-Narbat et al.^[20]. Briefly, the plates were immersed in 1 ml PBS (pH = 7.4) in the shaker incubator at 37°C for 3 days. At predetermined time intervals (1 h, 3 h, 5 h, 8 h, 12 h, 24 h, and 48 h) 500 µL of solution was removed and fresh PBS was replenished. The absorbance of sample solutions was measured at $\lambda_{\text{max}} = 280$ nm (the characteristic excitation wavelength for tryptophan). After calibrating the system with series of AMP standards, the AMP concentration was calculated based on the external standard method.

2.8. Cell study

MG-63 osteoblast-like cells, from National Cell Bank of Iran (NCBI) were cultured in Dulbecco's Modification of Eagles Medium (DMEM) consisting 10% fetal bovine serum (FBS), 100 U/ml penicillin, and 100 µg/ml streptomycin at 37°C under 95% humidified atmosphere and 5% CO₂. The culture medium was refreshed every 48 h. Triplicate specimens of (1) bare Ti (as control) (2) SF/HA-coated Ti and (3) SF/HA-coated Ti immobilized with HHC-36 implants were disinfected via dipping into ethanol, then immersing in PBS for 10 min three times.

For cell adhesion assay, 2×10^4 cells/cm² were cultured on samples in 24-well plate and maintained in the incubator. After 3 days, attached cells were fixed with 4% (v/v) glutaraldehyde solution, then rinsed with deionized water and finally dehydrated by 50%, 70%, 90%, and 100% alcohol solution, respectively. The dried specimens were gold sputter coated and observed under SEM.

The viability and proliferation of cells were evaluated by 3-(4,5-dimethylthiazol-2-yl)-2,5-diphenyltetrazolium-bromide assay kit (MTT)^[47]. In brief, MG-63 cells (5×10^3 cells/cm²) were seeded on samples and maintained in the incubator for 3 and 7 days. At each assigned day, the culture medium was replaced by 10 µl MTT solution (12 mM) and then kept in the incubator. After 4 h, 200 µl DMSO solution was added to each well to solubilize the formed purple formazan crystals. Eventually, absorbance was read at 570 nm using an ELISA Reader.

The Alkaline Phosphatase (ALP) expression of MG-63 cells, as an early stage osteoblast differentiation marker, was assessed based on our previous study^[48]. MG-63 cells (20×10^3 cell/cm²) were seeded on the plates for 3, 7, and 14 days. In order to discriminate between attached and non-attached cells to the surface of the culture plates, on one hand we put the samples on the plates so that they covered it completely and on the other hand, we added just 20 µl cells. At each time interval, the culture medium was completely removed and the adhered cells were lysed by 200 µl Radio Immuno Precipitation Assay lysis buffer (RIPA) and 2 µl Phenyl Methyl Sulfonyl Fluoride (PMSF) at 4°C. ALP activity was quantified according to ALP Elisa kit protocol and then normalized with the total protein concentration, which was measured by Bradford method. To find out the

amount of deposited calcium contents during 14 days of culture, 0.6 N HCl was added to the samples and after mixing thoroughly, total calcium content was measured according to the Arsenazo III kit Pars Azmoon manufacturer's instructions. Optical density was analyzed using the ELISA reader at 570 nm.

2.9. Antibacterial test

The antibacterial activity of the samples was measured using Bauer-Kirby Disk Diffusion method against both gram-negative *Escherichia coli* (*E. coli*) and gram-positive *Staphylococcus aureus* (*S. aureus*) bacteria. Briefly, some colonies of each strain were isolated and suspended in Nutrient Broth to prepare 0.5 McFarland standards. Afterward, 100 µl of the suspension was inoculated onto the nutrient agar plates and then the bare disinfected samples were placed on the plates^[20]. The plates were incubated at 37°C and after 24 h, the formed clear zones around the samples were measured. The colony-forming unit (CFU) was also measured to investigate the amount of viable cells at different times. Briefly, 400 µl of bacterial suspension with concentration of 1×10^6 CFU/ml was added to each disinfected specimen and then incubated at 37°C for 1 h, 2 h, and 3 h. Afterwards, 10 µl of residual bacteria was transferred to nutrient agar and incubated at 37°C. After 24 h, the number of bacterial colonies at each time was counted by UV Transilluminator^[19].

The bacterial growth on the AMP-treated plates was examined using SEM. In this regard, 50 µL of the bacterial suspension (1×10^6 cfu/ml) was incubated with the disinfected samples at 37°C for 24 h. Subsequently, samples were washed thoroughly with PBS, fixed with glutaraldehyde and dehydrated by graded alcohol solution before coating with the thin layer of gold^[27].

2.10. Long-term stability assay

The long-term stability of the HHC-36-immobilized plates was assessed using leaching process as reported by Kaiyang Lim and et al.^[36]. Briefly, the plates were soaked in PBS at 4°C for 21 days. At each time point, the 100 µl of PBS was extracted and subjected to 100 µl volume of 1×10^6 cfu/ml bacterial suspension and finally after 24 h the antimicrobial activity was assessed by Optical density (OD600) measurements.

2.11. Statistical analysis

All experimental data were analyzed by one-way ANOVA for comparison. * $p < 0.05$ and ** $p < 0.01$ were considered as significant and very significant, respectively.

3. Results and discussion

3.1. Characterization of nHA particles

SEM image (Figure 1a) shows the HA nanoparticles with average size of 27 ± 4.7 nm. Obtained EDX spectrum from

synthesized nHA indicates the Ca/P ratio of 1.56, close to the Ca/P ratio of the natural bone^[49](Figure 1b).

3.2. Characterization of SF/HA electrospun mats

Figure 2 depicts the SEM image, fibers diameter distribution, and EDX analysis of electrospun SF/HA mats. As expected, the beadless fibers (Figures 2a and 2b) with the diameter between 60 to 235 nm were observed. Maybe at first glance this seems a little wide, but if we consider the diagram, it is obvious that most distribution is in the range of 136-185 nm and the average diameter of the fibers was measured as 173 ± 15 nm. Moreover, because of ratio of HA/SF nanofibers seem smooth. The amount of Hydroxyapatite nanoparticles are too little to feature on nanofibers' morphology. EDS elemental mapping of Ca and P showed that both Ca and P were uniformly distributed in the electrospun mat (Figure 2c). This suggests that no HA agglomeration was observed in electrospun nanofibers. The FTIR spectra of the pure SF and SF/HA electrospun mats are shown in Figure 3. The characteristic peaks at 546 cm^{-1} and 1066 cm^{-1} and 1490 cm^{-1} are attributed to the vibration of PO_4^{3-} and CO_3^{2-} groups in HA. The appearance of these peaks

confirms that HA has formed in composite mat. Moreover, the peaks of the amide I (C=O stretching), amide II (N-H bending), and amide III (N-H bending and C-N stretching) in SF structure are located at 1655 cm^{-1} , 1535 cm^{-1} and 1234 cm^{-1} , respectively, which are attributed to the β -sheet structure of silk fibroin (silk II)^[14, 45, 46, 50, 51]. Appearance of these peaks in both of the SF and SF/HA mats after methanol treatment shows that incorporation of HA in SF structure has no influence on the SF structure as previously reported by other groups^[13]. Measurements of the pull-off forces show that adhesive strength between SF mat and Ti is about $2.07 \pm 0.2\text{ MPa}$ ($n=3$). Different factors such as physical forces between Ti implant and SF mat which are influenced by surface roughness, due to grounding and etching of Ti, and chemical forces such as hydrogen bridging bonds between oxide layer of Ti and SF nanofibers can affect the adhesion^[52].

The SEM morphology of electrospun SF/HA nanofibers after modification with PDA and HHC-36 is shown in Figure 4. As depicts, PDA with small spherical morphology is observed on the surface of electrospun fibers. The calculated mean fiber diameter is $181 \pm 12\text{ nm}$ in SF/HA/PDA and $193 \pm 15\text{ nm}$ in SF/HA/PDA/HHC-36. It is shown that

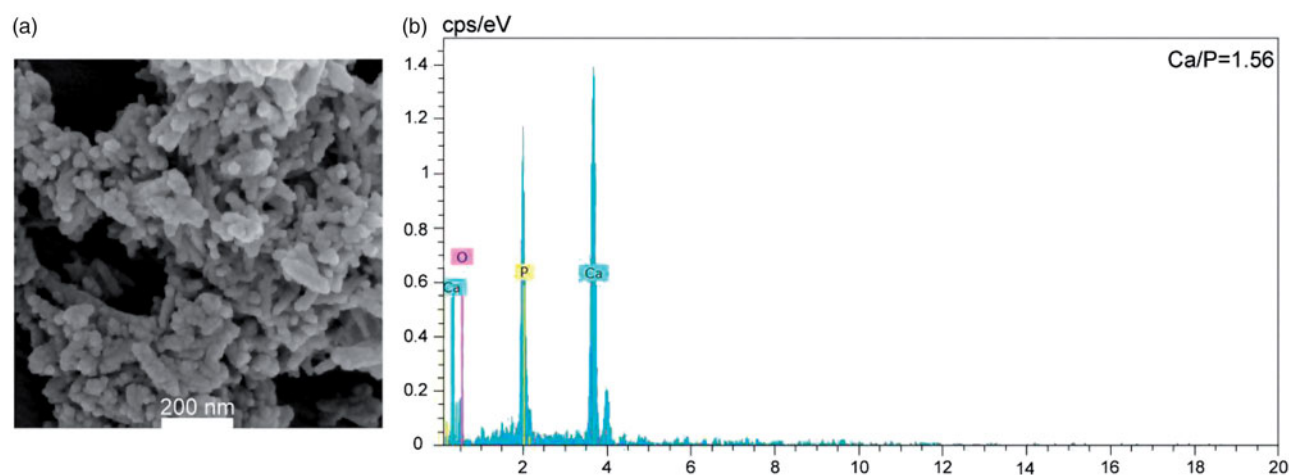


Figure 1. (a) FE-SEM image (b) EDX spectrum of HA nanoparticles.

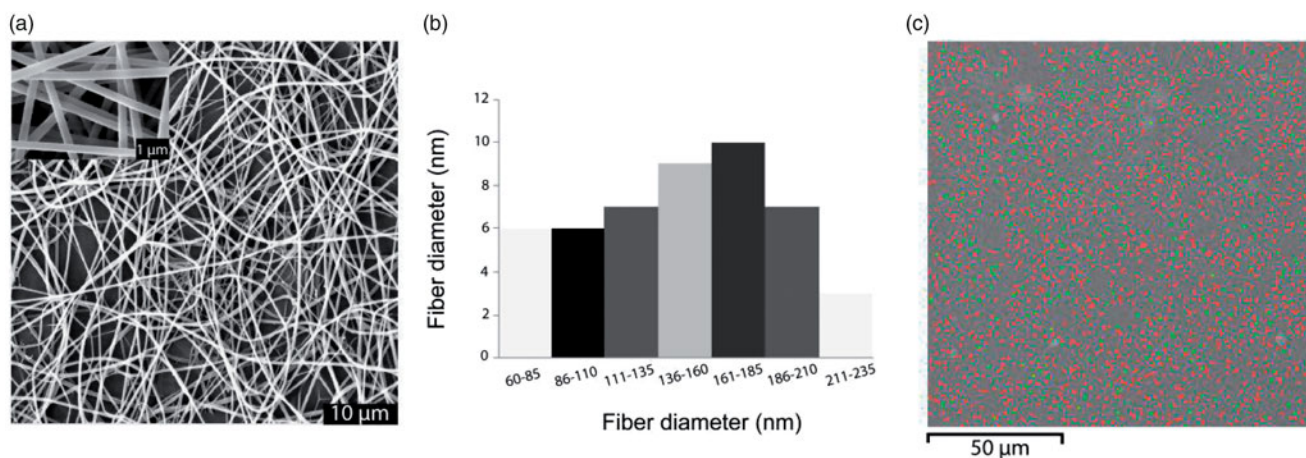


Figure 2. (a) SEM image of SF/HA electrospun nanofibers (b) fiber diameter distribution of the electrospun nanofibers (c) EDX image of SF nanofibers containing HA nanoparticles (Ca; red P; green).

loading PDA and HHC-36 on SF/HA electrospun mats has no significant effect on the average fiber diameter of SF/HA nanofibers ($p > 0.05$).

Table 1 indicates the water contact angle data of Ti plates before and after PDA and HHC-36 addition. It can be seen that the contact angle increases from $69.46^\circ \pm 2.2^\circ$ in bare Ti to $106.3^\circ \pm 1.2^\circ$ in SF/HA. This can be explained by the hydrophobic nature of silk II structure in electrospun SF/HA mats (Figure 3). However, modification of SF/HA nanofibers with PDA, significantly enhances the hydrophilicity of the implant surface and decreases the contact angle to 25.08° . This change is attributed to the presence of free amino groups on the SF/HA mats after physically adsorption of PDA catechol groups on the mats surface. Lowering the water contact angle of the hydrophobic surfaces after coating with PDA has been reported in previous studies^[36]. As summarized in Table 1, immobilizing HHC-36 on the SF/HA/PDA samples slightly increases the water contact angle as a result of its amphipathic nature.

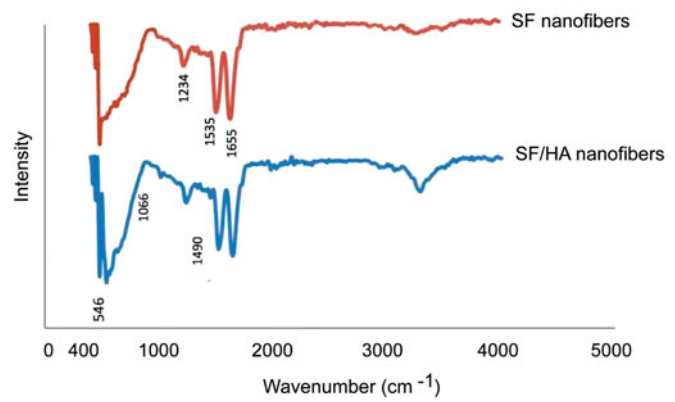


Figure 3. FTIR spectra of electrospun (a) SF and (b) SF/HA hybrid nanofibers.

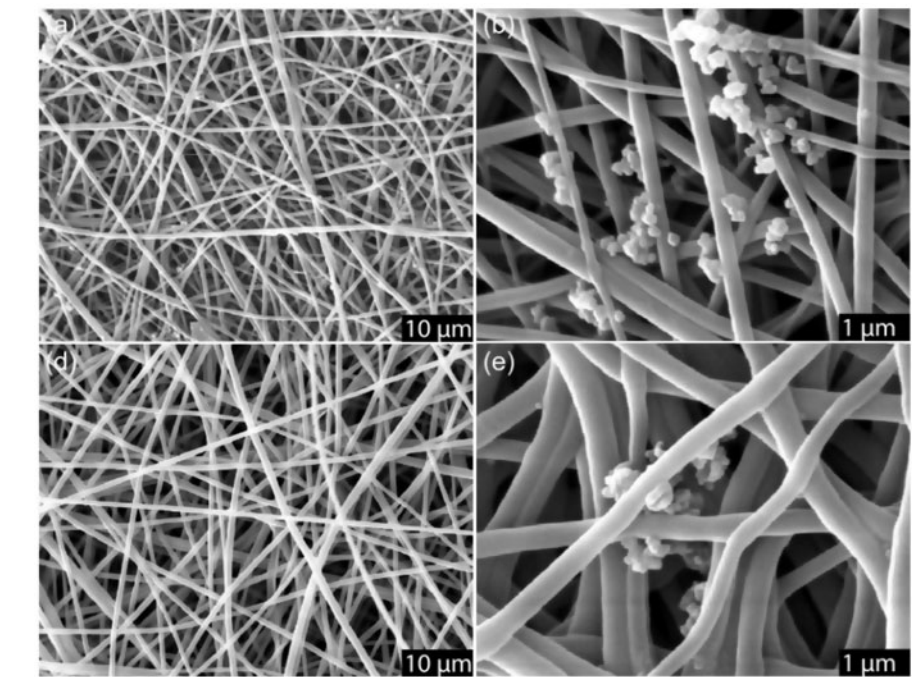


Figure 4. The SEM morphology and fiber diameter distribution of electrospun SF/HA nanofibers after modification with (a,b,c) PDA and (d,e,f) HHC-36.

Figure 5 shows the cumulative release profile of HHC-36 during 48 h soaking in PBS. It is evident that HHC-36 has a burst release during the first 3 h of soaking and then a slow steady release for 48 h. This suggests that the Ti plates share both of the burst and slow release of HHC-36 antimicrobial peptide. This release profile can be utilized in infection control, when a burst release of antibacterial agent within few hours is critical to eradicate bacteria following by slow steady release for few days to control the infection.

Table 1. Contact angle measurements of deionized water.

Surface	Photographs	Contact angle
Ti		69.46 ± 2.2
SF/HA		106.3 ± 1.2
SF/HA/PD		25.08 ± 2.4
SF/HA/PD/AMP		36.9 ± 1.8

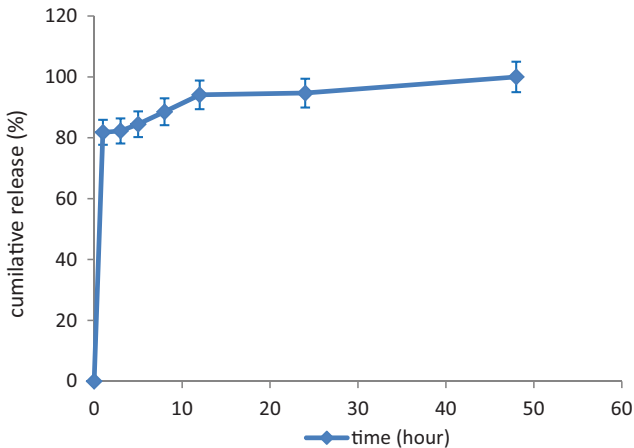


Figure 5. Cumulative release profile of HHC36 from SF/HA/AMP coated Ti.

3.3. Cell study

The morphology of MG-63 cells cultured on Ti, Ti/SF/HA, and Ti/SF/HA/AMP plates after 3 days is shown in Figure 6. Good cell attachment is observed in all groups (Figures 6a–c), however higher cell spread and cytoplasmic extension are observed on electrospun plates with and without AMP (Figures 6b and 6c). The colony shape of the cells of modified samples after 3 days approve the high rate of the cell proliferation on these implants. The results of the cell viability from direct MTT assay of all samples in comparison with the control group after 3 and 7 days are shown in Figure 7. No significant difference is observed in cellular viability of samples (Ti/SF/HA, and Ti/SF/HA/AMP) in compare to the control (Ti), which suggest a high cytocompatibility. As depicts, higher cell proliferation is observed for elctrospun-coated Ti rather than pure Ti plates. Moreover, the results show that HHC-36 loading has not statistically affected the cellular proliferation. The decrease in cellular proliferation on day 7th might be due to the inter-cellular contact inhibition mechanism^[53]. Both SEM and MTT results indicate that coating Ti plates with SF/HA nanometric fibers enhances cellular spreading and proliferation. This can be because of the higher surface area of nanometric fibers as well as its similarity to bone ECM structure. Recent studies show that using hybrid composites of polymeric nanofibers-HA have great potential in stimulating cellular responses and consequently improving osseointegration^[50].

Figures 8a and 8b depicts the ALP activity (as an early differentiation marker) and calcium content (matrix mineralization) of MG-63 cells cultured on studied Ti, Ti/SF/HA, and Ti/SF/HA/AMP implants during 14 days of culture. As shown in Figure 8a, the ALP activity reaches maximum at day 7th of culture and then decreases with increasing the incubation time. However, the ALP level is significantly higher in electrospun-coated samples in comparison with bare Ti plate ($p < 0.05$). This can be related to the greater proliferation of MG-63 cells on the plates containing electrospun samples. Previous studies mentioned that high cell density affects ALP activity and consequently mineralization^[54, 55]. In all samples, the calcium content increases over time (Figure 8b). However, this increase is considerably significant in plates consisting electrospun SF/HA after 14 days of culture, as expected. This is in agreement with previous studies showing that the down-regulation in ALP

expression is accompanied with increase upregulation of some osteogenic proteins, which enhanced ECM formation and consequently mineralization^[56].

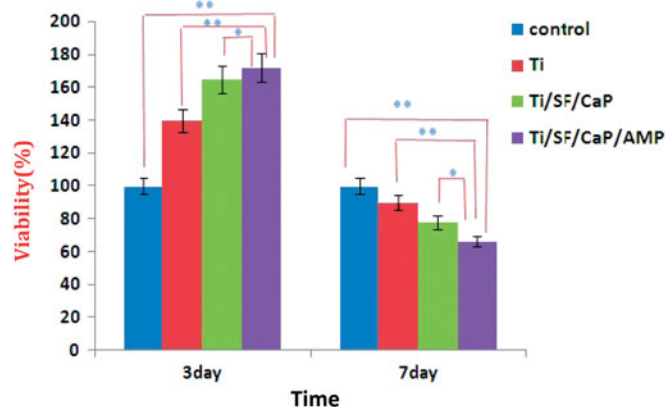


Figure 7. MTT assay performed to evaluate the viability of MG63 cells after exposed to Ti, Ti/SF/HA, and Ti/SF/HA/AMP.

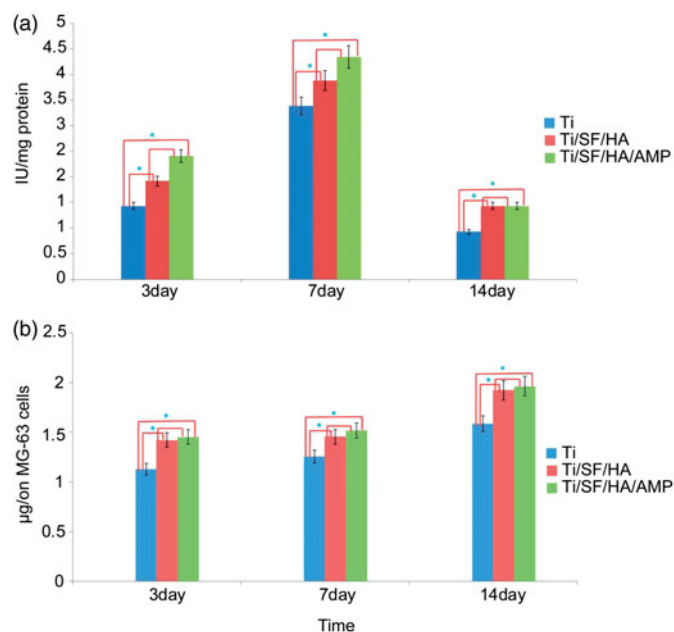


Figure 8. (a) The ALP activity and (b) Ca assay of MG-63 cells on Ti, Ti/SF/HA, and Ti/SF/HA/AMP during 14 days.

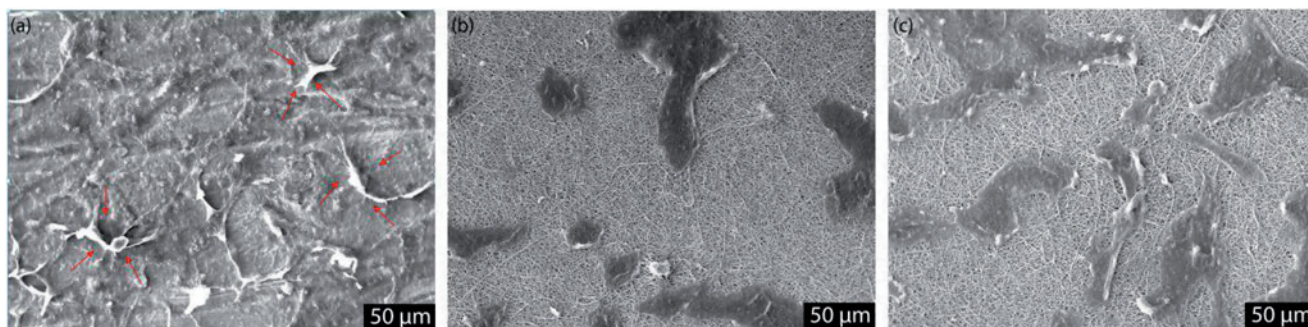


Figure 6. SEM image of morphology and cell attachment of MG-63 on (a) Ti (b) Ti/SF/HA and (c) Ti/SF/HA/AMP after 3 days.

3.4. Antimicrobial activity and stability of HHC-36 immobilized Ti plates

Figure 9 shows the inhibition zone formed by HHC-36 treated Ti plates against *E. coli* and *S. aureus* in comparison

with plates without HHC-36. As shown, the inhibition zone with diameter of 2.9 mm for *E. coli* and 2.1 mm for *S. aureus* appeared around the HHC-36 coated samples, while no inhibition zone was observed for both bare Ti and Ti/SF/HA plates. Moreover, the results of colony forming unit test

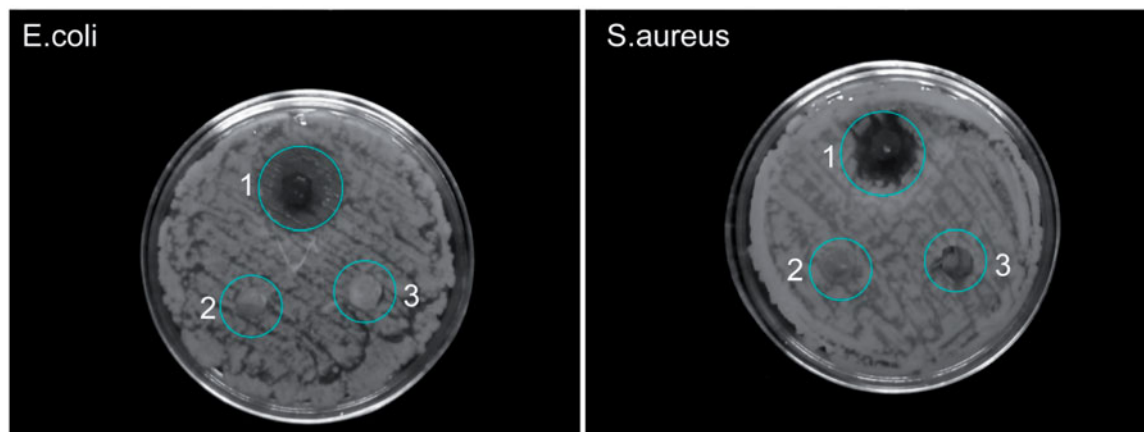


Figure 9. Assessing the antibacterial activity of (1) Ti/SF/HA/AMP (2) Ti/SF/HA and (3) Ti against *E. Coli* and *S. aureus* by Disk Diffusion test.

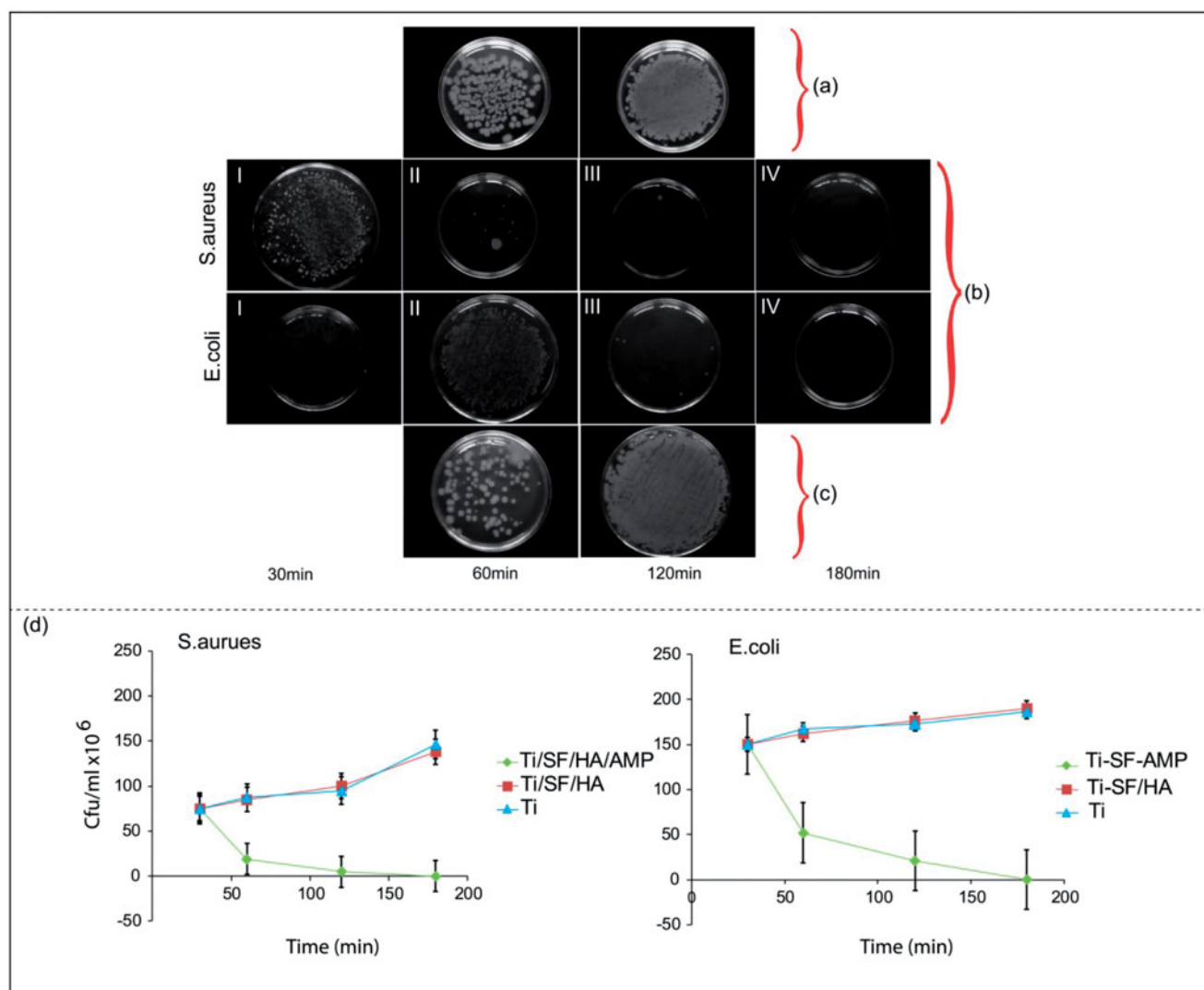


Figure 10. Antimicrobial activity of (a) Ti/SF/HA against *S. aureus* (b) Ti/SF/HA/AMP samples against *S. aureus* and *E. Coli* (c) Ti/SF/HA against *E. coli* and (d) diagram of bacteriacial ability in Ti/SF/HA/AMP samples against *S. aureus* and *E. Coli*.

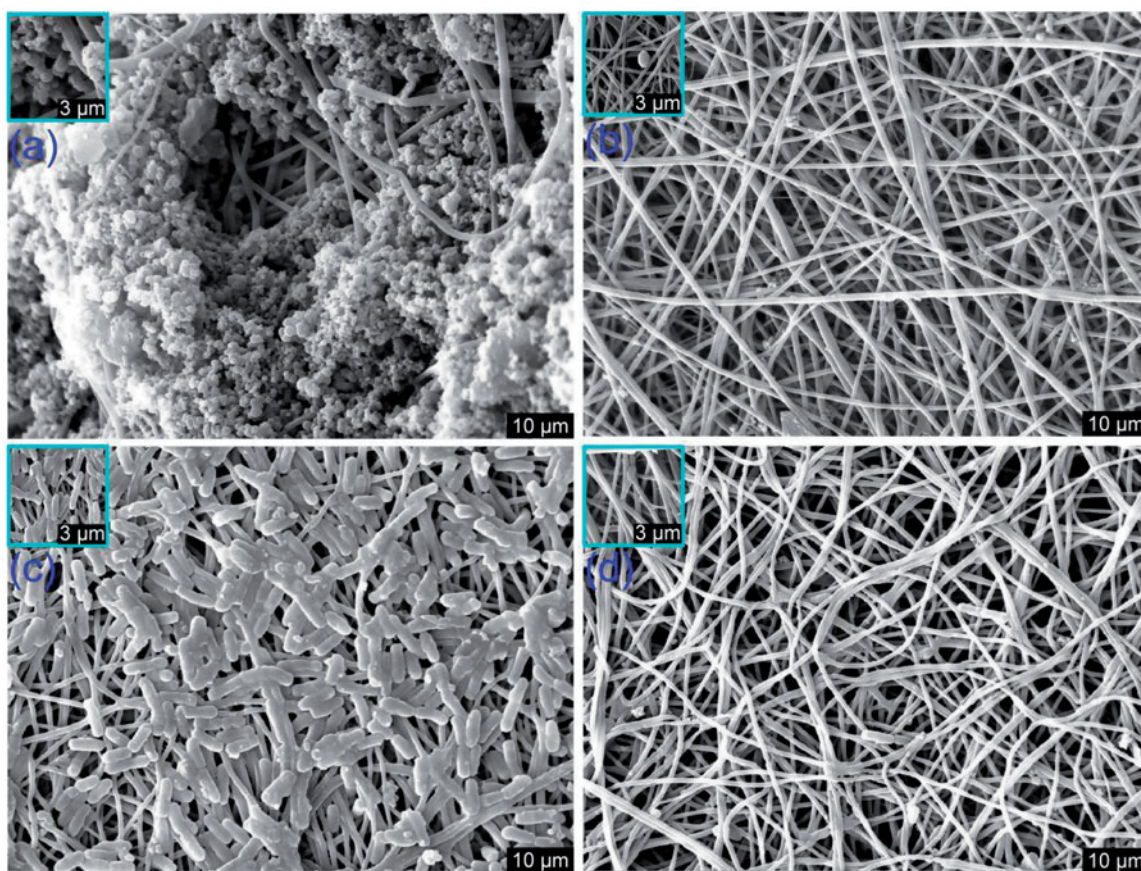


Figure 11. SEM images of *S. aureus* and *E. coli* bacteria incubated on the (a,c) Ti/SF/HA (b,d) Ti/SF/HA/AMP.

indicated 100% eradication of both gram-positive (*S. aureus*) and gram-negative (*E. coli*) bacteria after 3 h for the HHC-36 immobilized samples (Figure 10). Figure 11 shows the SEM images of overnight cultured *S. aureus* and *E. coli* on electrospun-coated Ti plates with and without HHC-36. As expected very few bacteria were detected on HHC-36 loaded samples, while a great number of bacteria were attached and agglomerated on Ti plates without HHC-36.

The obtained results clearly exhibited the bactericidal properties of HHC-36 against both *E. coli* and *S. aureus* after loading on Ti plates. This agrees with the previous studies regarding the high antibacterial activities of HHC-36 against the broad-spectrum of bacteria. A.Cherkasov et.al^[32] has reported that HHC-36 has low minimum inhibitory concentration (MIC) of 2.7 to 5.4 μM against *E. coli* and 1.4 to 2.9 μM against *S. aureus*, which is significantly lower than common antibiotics. It is believed that, the unique killing mechanism of the HHC-36 is based on the electrostatic interaction between positively charged group of HHC-36 ($\text{pI} = 12.3$) and negatively charged membrane of bacteria at physiological pH^[22, 57].

Figure 12 illustrates the long-term stability of HHC-36 to keep its antimicrobial activity. It was evident that in compare to the control samples, the absorbance of HHC-36-treated Ti plates at OD_{600} was significantly lower than non-treated plates. This suggests that the HHC-36-coated sample has maintained its antibacterial activities from days to weeks, which is essential for utilizing implanted materials.

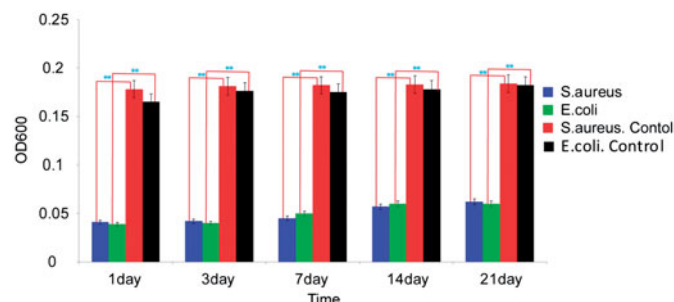


Figure 12. Stability of the (a) HHC-36-immobilized Ti implant and (b) Ti implant without HHC-36 over 21 days.

4. Conclusion

In this work, the silk fibroin/HA nanofibers were coated via electrospinning on Ti plate. The AMP HHC-36 was subsequently immobilized onto the coating using PDA, as a linker to create an antimicrobial coating on Ti. Characterization tests confirmed the inclusion and distribution of HA into silk fibroin and the morphology, bioactivity, and adhesive strength of designed implant were evaluated. The release profile of HHC-36 demonstrated a burst release of AMP within 3 h followed by a steady slow release for a few days. No cytotoxicity was observed on either of samples when cultured with MG-63 cells. The coated implants showed to be able to potentially enhance osteinductivity and mineralization. Finally, antimicrobial tests against *E. coli* and *S. aureus*

bacteria exhibited the ability of the proposed coating to eradicate the representative Gram-negative and Gram-positive bacteria and keep the inhibition ability for up to 21 days.

Acknowledgments

The corresponding author would like to acknowledge the financial support from the Faculty of New Sciences and Technologies, University of Tehran, Iran.

References

- [1] Long, M.; Rack, H. J. Titanium Alloys in Total Joint Replacement—a Materials Science Perspective. *Biomaterials* **1998**, *19*, 1621–1639. DOI: [10.1016/S0142-9612\(97\)00146-4](https://doi.org/10.1016/S0142-9612(97)00146-4).
- [2] Barrere, F.; Mahmood, T. A.; De Groot, K.; VanBlitterswijk, C. A. Advanced Biomaterials for Skeletal Tissue Regeneration: Instructive and Smart Functions. *Mater. Sci. Eng. R* **2008**, *59*, 38–71. DOI: [10.1016/j.mser.2007.12.001](https://doi.org/10.1016/j.mser.2007.12.001).
- [3] Kuroda, D.; Niinomi, M.; Morinaga, M.; Kato, Y.; Yashiro, T.; Niinomi, M.; Morinaga, M.; Kato, Y.; Ashiro, T.Y. Design and Mechanical Properties of New β Type Titanium Alloys for Implant Materials. *Mater. Sci. Eng. A* **1998**, *243*, 244–249. DOI: [10.1016/S0921-5093\(97\)00808-3](https://doi.org/10.1016/S0921-5093(97)00808-3).
- [4] Lim, J. I.; Yu, B.; Woo, K. M.; Lee, Y. K. Immobilization of TiO₂ Nanofibers on Titanium Plates for Implant Applications. *Appl. Surf. Sci.* **2008**, *255*, 2456–2460. DOI: [10.1016/j.apsusc.2008.07.146](https://doi.org/10.1016/j.apsusc.2008.07.146).
- [5] de Andrade, D. P.; de Vasconcellos, L. M. R.; Carvalho, I. C. S.; Forte, L. F. D. B. P.; de Souza Santos, E. L.; do Prado, R. F.; dos Santos, D. R.; Alves Cairo, C. A.; Carvalho, Y. R. Titanium–35niobium Alloy as a Potential Material for Biomedical Implants: In Vitro Study. *Mater. Sci. Eng. C* **2015**, *56*, 538–544. DOI: [10.1016/j.msec.2015.07.026](https://doi.org/10.1016/j.msec.2015.07.026).
- [6] Bajgai, M. P.; Parajuli, D. C.; Park, S. J.; Chu, K. H.; Kang, H. S.; Kim, H. Y. Hydroxyapatite Particulate Nanofiber Modified Titanium: In-Vitro Bioactivity. *Bioceram. Dev. Appl.* **2010**, *1*, 4. DOI: [10.4303/bda/D110131](https://doi.org/10.4303/bda/D110131).
- [7] Im, K. H.; Lee, S. B.; Kim, K. M.; Lee, Y. K. Improvement of Bonding Strength to Titanium Surface by Sol–Gel Derived Hybrid Coating of Hydroxyapatite and Titania by Sol–Gel Process. *Surf. Coat. Technol.* **2007**, *202*, 1135–1138. DOI: [10.1016/j.surfcoat.2007.07.081](https://doi.org/10.1016/j.surfcoat.2007.07.081).
- [8] Li, Y.; Lee, I. S.; Cui, F. Z.; Choi, S. H. The Biocompatibility of Nanostructured Calcium Phosphate Coated on Micro-Arc Oxidized Titanium. *Biomaterials* **2008**, *29*, 2025–2032. DOI: [10.1016/j.biomaterials.2008.01.009](https://doi.org/10.1016/j.biomaterials.2008.01.009).
- [9] Jaya, S.; Durance, T. D.; Wang, R. Preparation and Physical Characterization of Gelatin–Starch/Hydroxyapatite Porous Composite Scaffold Fabricated Using Novel Microwave Energy under Vacuum Technique. *J. Compos. Mater.* **2009**, *43*, 1451–1460. DOI: [10.1177/0021998308105432](https://doi.org/10.1177/0021998308105432).
- [10] Luong, N. D.; Moon, I. S.; Nam, J. D. A Solvent-Assisted Compression Molded of Poly (L-Lactide)/Hydroxyapatite Electrospun Fibers for Robust Engineered Scaffold Systems. *Macromol. Mater. Eng.* **2009**, *294*, 699–704. DOI: [10.1002/mame.200900204](https://doi.org/10.1002/mame.200900204).
- [11] Lee, H. J.; Lee, S. J.; Uthaman, S.; Thomas, R. G.; Hyun, H.; Jeong, Y. Y.; Cho, C. S.; Park, I. K. Biomedical Applications of Magnetically Functionalized Organic/Inorganic Hybrid Nanofibers. *IJMS* **2015**, *16*, 13661–13677. DOI: [10.3390/ijms160613661](https://doi.org/10.3390/ijms160613661).
- [12] Mottaghtalab, F.; Hosseinkhani, H.; Shokrgozar, M. A.; Mao, C.; Yang, M.; Farokhi, M. Silk as a Potential Candidate for Bone Tissue Engineering. *J Control Release* **2015**, *215*, 112–128. DOI: [10.1016/j.jconrel.2015.07.031](https://doi.org/10.1016/j.jconrel.2015.07.031).
- [13] Sheikh, F. A.; Ju, H. W.; Moon, B. M.; Park, H. J.; Kim, J. H.; Lee, O. J.; Park, C.H. A Novel Approach to Fabricate Silk Nanofibers Containing Hydroxyapatite Nanoparticles Using a Three-Way Stopcock. *Nanoscale. Res. Lett.* **2013**, *8*, 303.
- [14] Wei, K.; Li, Y.; Kim, K. O.; Nakagawa, Y.; Kim, B. S.; Abe, K.; Chen, G. Q.; Kim, I. S. Fabrication of Nano-Hydroxyapatite on Electrospun Silk Fibroin Nanofiber and Their Effects in Osteoblastic Behavior. *J. Biomed. Mater. Res.* **2011**, *97*, 272–280. DOI: [10.1002/jbm.a.33054](https://doi.org/10.1002/jbm.a.33054).
- [15] Lee, D.-W.; Yun, Y.-P.; Park, K.; Kim, S. E.; YunPark, Y.P.K.; Kim, S.E. Gentamicin and Bone Morphogenic Protein-2 (BMP-2)-Delivering Heparinized-Titanium Implant with Enhanced Antibacterial Activity and Osteointegration. *Bone* **2012**, *50*, 974–982.
- [16] Gimeno, M.; Pinczowski, P.; Pérez, M.; Giorello, A.; Martínez, M. Á.; Santamaría, J.; Arruebo, M.; Luján, L. A Controlled Antibiotic Release System to Prevent Orthopedic-Implant Associated Infections: An in Vitro. *Eur. J. Pharm. Biopharm.* **2015**, *96*, 264–271. DOI: [10.1016/j.ejpb.2015.08.007](https://doi.org/10.1016/j.ejpb.2015.08.007).
- [17] Zhang, F.; Zhang, Z.; Zhu, X.; Kang, E. T.; Neoh, K. G. Silk-Functionalized Titanium Surfaces for Enhancing Osteoblast Functions and Reducing Bacterial Adhesion. *Biomaterials* **2008**, *29*, 4751–4759. DOI: [10.1016/j.biomaterials.2008.08.043](https://doi.org/10.1016/j.biomaterials.2008.08.043).
- [18] Goodman, S. B.; Yao, Z.; Keeney, M.; Yang, F. The Future of Biologic Coatings for Orthopaedic Implants. *Biomaterials* **2013**, *34*, 3174–3183. DOI: [10.1016/j.biomaterials.2013.01.074](https://doi.org/10.1016/j.biomaterials.2013.01.074).
- [19] Kazemzadeh-Narbat, M.; Kindrachuk, J.; Duan, K.; Jenssen, H.; Hancock, R. E.; Wang, R. Antimicrobial Peptides on Calcium Phosphate-Coated Titanium for the Prevention of Implant-Associated Infections. *Biomaterials* **2010**, *31*, 9519–9526. DOI: [10.1016/j.biomaterials.2010.08.035](https://doi.org/10.1016/j.biomaterials.2010.08.035).
- [20] Kazemzadeh-Narbat, M.; Lai, B. F.; Ding, C.; Kizhakkedathu, J. N.; Hancock, R. E.; Wang, R. Multilayered Coating on Titanium for Controlled Release of Antimicrobial Peptides for the Prevention of Implant-Associated Infections. *Biomaterials* **2013**, *34*, 5969–5977. DOI: [10.1016/j.biomaterials.2013.04.036](https://doi.org/10.1016/j.biomaterials.2013.04.036).
- [21] El-Azizi, M.; Rao, S.; Kanchanapoom, T.; Khardori, N. In Vitro Activity of Vancomycin, Quinupristin/Dalfopristin, and Linezolid against Intact and Disrupted Biofilms of Staphylococci. *Ann. Clin. Microbiol. Antimicrob.* **2005**, *4*, 2. DOI: [10.1186/1476-0711-4-2](https://doi.org/10.1186/1476-0711-4-2).
- [22] Kazemzadeh-Narbat, M.; Noordin, S.; Masri, B. A.; Garbuz, D. S.; Duncan, C. P.; Hancock, R. E.; Wang, R. Drug Release and Bone Growth Studies of Antimicrobial Peptide-Loaded Calcium Phosphate Coating on Titanium. *J. Biomed. Mater. Res.* **2012**, *100*, 1344–1352. DOI: [10.1002/jbm.b.32701](https://doi.org/10.1002/jbm.b.32701).
- [23] Tunney, M. M.; Ramage, G.; Patrick, S.; Nixon, J. R.; Murphy, P. G.; Gorman, S. P. Antimicrobial Susceptibility of Bacteria Isolated from Orthopedic Implants following Revision Hip Surgery. *Antimicrob. Agents Chemother.* **1998**, *42*, 3002–3005. DOI: [10.1128/AAC.42.11.3002](https://doi.org/10.1128/AAC.42.11.3002).
- [24] Bai, L.; Zhu, L.; Min, S.; Liu, L.; Cai, Y.; Yao, J. Surface Modification and Properties of Bombyxmori Silk Fibroin Films by Antimicrobial Peptide. *Appl. Surf. Sci.* **2008**, *254*, 2988–2995. DOI: [10.1016/j.apsusc.2007.10.049](https://doi.org/10.1016/j.apsusc.2007.10.049).
- [25] Han, F. F.; Liu, Y. F.; Xie, Y. G.; Gao, Y. H.; Luan, C.; Wang, Y. Z. Antimicrobial Peptides Derived from Different Animals: comparative Studies of Antimicrobial Properties, Cytotoxicity and Mechanism of Action. *World J. Microbiol. Biotechnol.* **2011**, *27*, 1847–1857. DOI: [10.1007/s11274-010-0643-9](https://doi.org/10.1007/s11274-010-0643-9).
- [26] Aoki, W.; Ueda, M. Characterization of Antimicrobial Peptides toward the Development of Novel Antibiotics. *Pharmaceuticals* **2013**, *6*, 1055–1081. DOI: [10.3390/ph6081055](https://doi.org/10.3390/ph6081055).
- [27] Song, D. W.; Kim, S. H.; Kim, H. H.; Lee, K. H.; Ki, C. S.; Park, Y. H. Multi-Biofunction of Antimicrobial Peptide-Immobilized Silk Fibroin Nanofiber Membrane: Implications for Wound Healing. *Acta. Biomater.* **2016**, *39*, 146–155. DOI: [10.1016/j.actbio.2016.05.008](https://doi.org/10.1016/j.actbio.2016.05.008).
- [28] Nichols, M.; Kuljanin, M.; Nategholeslam, M.; Hoang, T.; Vafaei, S.; Tomberli, B.; Gray, C. G.; DeBruin, L.; Jelokhani-

- Niaraki, M. Dynamic Turn Conformation of a Short Tryptophan-Rich Cationic Antimicrobial Peptide and Its Interaction with Phospholipid Membranes. *J. Phys. Chem. B* **2013**, *117*, 14697–14708. DOI: [10.1021/jp4096985](https://doi.org/10.1021/jp4096985).
- [29] Glukhov, E.; Stark, M.; Burrows, L. L.; Deber, C. M. Basis for Selectivity of Cationic Antimicrobial Peptides for Bacterial versus Mammalian Membranes. *J. Biol. Chem.* **2005**, *280*, 33960–33967. DOI: [10.1074/jbc.M507042200](https://doi.org/10.1074/jbc.M507042200).
- [30] Powers, J. P. S.; Hancock, R. E. The Relationship between Peptide Structure and Antibacterial Activity. *Peptides* **2003**, *24*, 1681–1691. DOI: [10.1016/j.peptides.2003.08.023](https://doi.org/10.1016/j.peptides.2003.08.023).
- [31] Vafaei, S. A Molecular Dynamics Simulation-Isothermal Titration Calorimetry Study of Antimicrobial Peptide-Peptide Interaction, **2015**.
- [32] Cherkasov, A.; Hilpert, K.; Jenssen, H.; Fjell, C. D.; Waldbrook, M.; Mullaly, S. C.; Volkmer, R.; Hancock, R. E. Use of Artificial Intelligence in the Design of Small Peptide Antibiotics Effective against a Broad Spectrum of Highly Antibiotic-Resistant Superbugs. *Acs Chem. Biol.* **2009**, *4*, 65–74. DOI: [10.1021/cb800240j](https://doi.org/10.1021/cb800240j).
- [33] Cheng, H.; Yue, K.; Kazemzadeh-Narbat, M.; Liu, Y.; Khalilpour, A.; Li, B.; Zhang, Y. S.; Annabi, N.; Khademhosseini, A. Mussel-Inspired Multifunctional Hydrogel Coating for Prevention of Infections and Enhanced Osteogenesis. *ACS Appl. Mater. Interfaces* **2017**, *9*, 11428–11439.
- [34] Bagheri, M.; Beyermann, M.; Dathe, M. Immobilization Reduces the Activity of Surface-Bound Cationic Antimicrobial Peptides with No Influence upon the Activity Spectrum. *Antimicrob. Agents. Chemother.* **2009**, *53*, 1132–1141. DOI: [10.1128/AAC.01254-08](https://doi.org/10.1128/AAC.01254-08).
- [35] Gabriel, M.; Nazmi, K.; Veerman, E. C.; Nieuw Amerongen, A. V.; Zentner, A. Preparation of LL-37-Grafted Titanium Surfaces with Bactericidal Activity. *Bioconjugate. Chem.* **2006**, *17*, 548–550. DOI: [10.1021/bc050091v](https://doi.org/10.1021/bc050091v).
- [36] Lim, K.; Chua, R. R. Y.; Ho, B.; Tambyah, P. A.; Hadinoto, K.; Leong, S. S. J. Development of a Catheter Functionalized by a Polydopamine Peptide Coating with Antimicrobial and Antibiofilm Properties. *Acta. Biomater.* **2015**, *15*, 127–138. DOI: [10.1016/j.actbio.2014.12.015](https://doi.org/10.1016/j.actbio.2014.12.015).
- [37] Eriksen, T. H. B.; Skovsen, E.; Fojan, P. Release of Antimicrobial Peptides from Electrospun nanofibres as a Drug Delivery System. *J. Biomed. Nanotechnol.* **2013**, *9*, 492–498. DOI: [10.1166/jbn.2013.1553](https://doi.org/10.1166/jbn.2013.1553).
- [38] Rabiei, M.; Sabahi, H.; Rezayan, A. H. Gallic Acid-Loaded Mont-Morillonite Nanostructure as a New Controlled Release System. *Appl. Clay. Sci.* **2016**, *119*, 236–242. DOI: [10.1016/j.clay.2015.10.020](https://doi.org/10.1016/j.clay.2015.10.020).
- [39] Rezayan, A. H.; Mousavi, M.; Kheirjou, S.; Amoabediny, G.; Ardestani, M. S.; Mohammadnejad, J. Monodisperse Magnetite (Fe₃O₄) Nanoparticles Modified with Water Soluble Polymers for the Diagnosis of Breast Cancer by MRI Method. *J. Magn. Magnetic. Mater.* **2016**, *420*, 210–217. DOI: [10.1016/j.jmmm.2016.07.003](https://doi.org/10.1016/j.jmmm.2016.07.003).
- [40] Oroojalian, F.; Rezayan, A. H.; Shier, W. T.; Abnous, K.; Ramezani, M. Megalin-Targeted Enhanced Transfection Efficiency in Cultured Human HK-2 Renal Tubular Proximal Cells Using Aminoglycoside-Carboxyalkyl-Polyethylenimine-Containing Nanoplexes. *Inter. J. Pharmaceutics.* **2017**, *523*, 102–120.
- [41] Taheri, R. A.; Rezayan, A. H.; Rahimi, F.; Mohammadnejad, J.; Kamali, M. Development of an Immunosensor Using Oriented Immobilized anti-OmpW for Sensitive Detection of *Vibrio cholerae* by Surface Plasmon Resonance. *Biosens. Bioelectron.* **2016**, *86*, 484–488. DOI: [10.1016/j.bios.2016.07.006](https://doi.org/10.1016/j.bios.2016.07.006).
- [42] Cho, H.-j.; Madhurakkat Perikamana, S. K.; Lee, J.-h.; Lee, J.; Lee, K.-M.; Shin, C. S.; Shin, H. Effective Immobilization of BMP-2 Mediated by Polydopamine Coating on Biodegradable Nanofibers for Enhanced in Vivo Bone Formation. *ACS Appl. Mater. Interfaces.* **2014**, *6*, 11225–11235. DOI: [10.1021/am501391z](https://doi.org/10.1021/am501391z).
- [43] Lee, H.; Dellatore, S. M.; Miller, W. M.; Messersmith, P. B. Mussel-Inspired Surface Chemistry for Multifunctional Coatings. *Science* **2007**, *318*, 426–430. DOI: [10.1126/science.1147241](https://doi.org/10.1126/science.1147241).
- [44] Gshalaev, V. S.; Demirchan, A. C. *Synthesis, Properties, and Applications of Hydroxyapatite*. Nova Science Publishers: Hauppauge, USA, **2012**.
- [45] Zadegan, S.; Hosainilipour, M.; Rezaie, H. R.; Ghassai, H.; Shokrgozar, M. A. Synthesis and Biocompatibility Evaluation of Cellulose/Hydroxyapatite Nanocomposite Scaffold in 1-n-Allyl-3-Methylimidazolium Chloride. *Mater. Sci. Eng. C* **2011**, *31*, 954–961.
- [46] Hadisi, Z.; Nourmohammadi, J.; Mohammadi, J. Composite of Porous Starch-Silk Fibroin Nanofiber-Calcium Phosphate for Bone Regeneration. *Ceram. Int.* **2015**, *41*, 10745–10754. DOI: [10.1016/j.ceramint.2015.05.010](https://doi.org/10.1016/j.ceramint.2015.05.010).
- [47] Ghaee, A.; Nourmohammadi, J.; Danesh, P. Novel Chitosan-Sulfonated Chitosan-Polycaprolactone-Calcium Phosphate Nanocomposite Scaffold. *Carbohydr. Polym.* **2017**, *157*, 695–703. DOI: [10.1016/j.carbpol.2016.10.023](https://doi.org/10.1016/j.carbpol.2016.10.023).
- [48] Shahriarpanah, S.; Nourmohammadi, J.; Amoabediny, G. Fabrication and Characterization of Carboxylated Starch-Chitosan Bioactive Scaffold for Bone Regeneration. *Int. J. Biol. Macromol.* **2016**, *93*, 1069–1078. DOI: [10.1016/j.ijbiomac.2016.09.045](https://doi.org/10.1016/j.ijbiomac.2016.09.045).
- [49] Sagadevan, S.; Dakshnamoorthy, A. Synthesis and Characterization of Nano-Hydroxyapatite (n-HAP) Using the Wet Chemical Technique. *Int. J. Phys. Sci.* **2013**, *8*, 1639–1645.
- [50] Ming, J.; Zuo, B. A Novel Electrospun Silk Fibroin/Hydroxyapatite Hybrid Nanofibers. *Mater. Chem. Phys.* **2012**, *137*, 421–427. DOI: [10.1016/j.matchemphys.2012.10.001](https://doi.org/10.1016/j.matchemphys.2012.10.001).
- [51] Nourmohammadi, J.; Shahriarpanah, S.; Asadzadeh-zanjani, N.; Khaleghpanah, S.; Heidari, S. Biomimetic Apatite Layer Formation on a Novel Citrate Starch Scaffold Suitable for Bone Tissue Engineering Applications. *Starch-Stärke* **2016**, *68*, 1275–1281. DOI: [10.1002/star.201500216](https://doi.org/10.1002/star.201500216).
- [52] Butt, M. A.; Chughtai, A.; Ahmad, J.; Ahmad, R.; Majeed, U.; Khan, I. H. Theory of Adhesion and Its Practical Implications. *JFET* **2008**, *1*, 21–45.
- [53] Gérard, C.; Goldbeter, A. The Balance between Cell Cycle Arrest and Cell Proliferation: control by the Extracellular Matrix and by Contact Inhibition. *Inter. Face. Focus* **2014**, *4*, 1–12.
- [54] Farokhi, M.; Mottaghtalab, F.; Hadjati, J.; Omidvar, R.; Majidi, M.; Amanzadeh, A.; Azami, M.; Tavangar, S. M.; Ai, J. Structural and Functional Changes of Silk Fibroin Scaffold Due to Hydrolytic Degradation. *J. Appl. Polym. Sci.* **2014**, *31*, 1–8.
- [55] Park, S. H.; Gil, E. S.; Shi, H.; Kim, H. J.; Lee, K.; Kaplan, D. L. Relationships between Degradability of Silk Scaffolds and Osteogenesis. *Biomaterials* **2010**, *31*, 6162–6172. DOI: [10.1016/j.biomaterials.2010.04.028](https://doi.org/10.1016/j.biomaterials.2010.04.028).
- [56] Koroleva, A.; Deiwick, A.; Nguyen, A.; Schlie-Wolter, S.; Narayan, R.; Timashev, P.; Popov, V.; Bagratashvili, V.; Chichkov, B. Osteogenic Differentiation of Human Mesenchymal Stem Cells in 3-D Zr-Si Organic-Inorganic Scaffolds Produced by Two-Photon Polymerization Technique. *PLoS One* **2015**, *10*, 1–18.
- [57] Kazemzadeh-Narbat, M.; Wang, Q.; Hancock, R. E.; Wang, R. Antimicrobial Peptide Delivery from Trabecular Bone Grafts. *J. Biomater. Tissue Eng.* **2014**, *4*, 967–972. DOI: [10.1166/jbt.2014.1272](https://doi.org/10.1166/jbt.2014.1272).